Mesoporous Organosilica

DOI: 10.1002/anie.201105394

Mesoporous Organosilica Hybrids Consisting of Silica-Wrapped π–π Stacking Columns**

Norihiro Mizoshita, Takao Tani, Hiroshi Shinokubo, and Shinji Inagaki**

Periodic mesoporous organosilica (PMO) materials prepared by surfactant-directed polycondensation of bridged organosilane precursors ($R[Si(OR')_3]_n$; $n \geq 2$, R = organic bridging groups, R′ = methyl, ethyl, etc.) are a new class of functional porous hybrid materials.[1–6] Organic groups R can be densely embedded within the pore walls without plugging the mesopores. Various organic bridges R ranging from functional π systems to metal complexes are available for tailoring functional frameworks with particular properties, such as tuning of HOMO–LUMO levels, fixation of electroactive organic groups, and formation of reactive and catalytic sites.[7–12] One of the most remarkable features of PMOs is the induction of molecular-scale periodicity in the pore wall, which has been realized for PMOs synthesized from dipodal rod-like precursors with rigid π-conjugated aromatic bridges (for example, 1,4-phenylene and 4,4′-biphenylylene) under basic hydrolytic conditions (Figure 1a, left).[13–20] Molecular-scale "crystal-like" ordering of the framework should enable design and control of the optical, electrical, and surface properties of PMOs. However, all of the conventional crystal-like PMOs show lamellar structures consisting of alternating organic and silica layers (Figure 1a, left).[13–20] In this configuration, the distance between neighboring organic bridges is about 0.44 nm, which is much longer than typical face-to-face π–π stacking distances (0.34–0.36 nm);[21,22] therefore, neither strong electronic coupling nor significant electroconductive properties are expected for the pore walls. The lamellar arrangement is thought to be directed by a hydrophobic–hydrophilic interaction of fully hydrolyzed dipodal precursors ($(HO)_3Si{-}R{-}Si(OH)_3$) and subsequent polycondensation; the position and distance of the organic bridges are restricted by the chemical bond length of the siloxane network.

Herein we present the first synthesis of a new class of molecularly ordered PMOs with columnar stacking of the bridging organic groups with a face-to-face π-stacking distance of 0.35–0.36 nm (Figure 1a, right). The new PMOs were synthesized by surfactant-directed polycondensation of newly designed disk-like alkoxysilane precursors with hydrophobic and electroactive perylene bisimide (PBI)[22] cores (Figure 1b). The key to the formation of this new type of the ordered structure is full utilization of the π–π stacking nature of the hydrophobic PBI moieties rather than the hydrophobic–hydrophilic interaction. As shown in Figure 1c, the formation of mesostructured hybrids consisting of π-stacked PBI columns and micellar aggregates of a cationic surfactant is promoted under basic hydrolytic conditions through columnar self-assembly of disk-like PBI precursors and electrostatic interaction between the cationic surface of the micelles and the anionic silanolate groups of the column-assembled precursors. The PBI columns are then wrapped and reinforced with a pure silica coating. Finally, the template surfactants are removed, resulting in mesoporous hybrids with pore walls consisting of silica-wrapped PBI columns. The π-stacked columnar channels within the pore walls should function as molecular wires and facilitate transport of charge, energy, and spin along the wires.[21,22] Such a molecular wire framework may be conductive to enhancement of charge separation and suppression of undesired charge recombination in photocatalytic reactions, as well as electronic applications. Moreover, electron-deficient PBI–silica hybrids can be regarded as electron acceptor assemblies; they are expected to function as an electron buffer for photochemical reactions involving photoinduced redox cycles.

We prepared two types of PBI precursor, PBI-3Pn-SiME and PBI-MEE-SiME (Figure 1b), with four bulky, polar, and flexible alkoxysilyl groups and different substituents (branched 3-pentyl (3Pn) and linear 2-(2-methoxyethoxy)-ethyl (MEE) groups) on the imide groups. These compounds were obtained by the recently developed ruthenium-catalyzed direct 2,5,8,11-alkylation of PBI with vinylsilane compounds (Supporting Information, Schemes S1 and S2).[23]

Mesostructured PBI–silica hybrids were obtained as dark solids by basic hydrolysis and condensation of the precursors PBI-3Pn-SiME and PBI-MEE-SiME in the presence of a cationic template surfactant (trimethyloctadecylammonium chloride). Figure 2a and b show X-ray diffraction (XRD) patterns of the surfactant-containing as-made hybrids, denoted as PBI-3Pn-PMO-am and PBI-MEE-PMO-am, respectively. The intense peaks at $2\theta \approx 2°$ indicate the formation of periodic mesostructures. While PBI-3Pn-PMO-

[*] Dr. N. Mizoshita, Dr. T. Tani, Dr. S. Inagaki
Toyota Central R&D Laboratories, Inc.
Nagakute, Aichi 480-1192 (Japan)
and
CREST, Japan Science and Technology Agency (JST)
Kawaguchi, Saitama 332-0012 (Japan)
E-mail: nmizoshita@mosk.tytlabs.co.jp
inagaki@mosk.tytlabs.co.jp
Prof. H. Shinokubo
Department of Applied Chemistry
Graduate School of Engineering, Nagoya University
Chikusa, Nagoya 464-8603 (Japan)

[**] We are grateful to Yoshifumi Aoki for the ESR measurements. We thank Dr. Yasutomo Goto and Dr. Tetsu Ohsuna for TEM observations. We also acknowledge Soichi Shirai, Dr. Masafumi Oda, Dr. Minoru Waki, and Yoshifumi Maegawa for helpful discussions.

Supporting information for this article is available on the WWW under http://dx.doi.org/10.1002/anie.201105394.

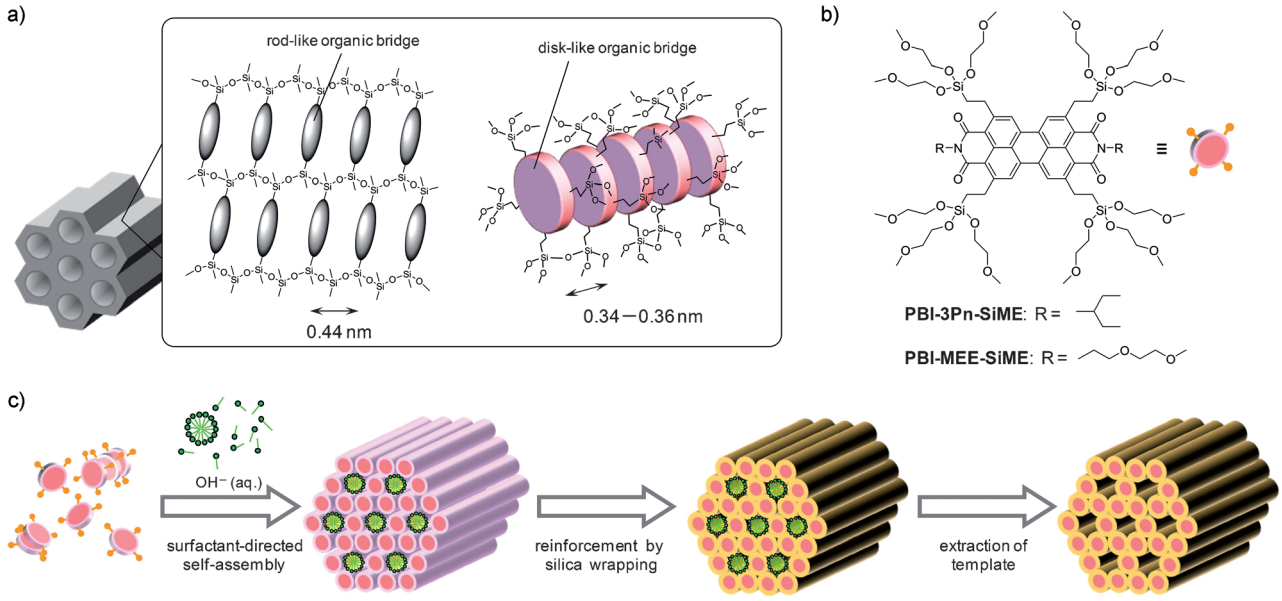

Figure 1. a) Illustration of molecularly ordered organosilica frameworks of PMOs with rod-like (left) and disk-like (right) organic bridges. b) Chemical structures of PBI-derived precursors. c) Preparation of PMO hybrids from disk-like PBI precursors.

am had a single peak at $d = 4.55$ nm, PBI-MEE-PMO-am had a diffraction peak at $d = 4.60$ nm with two weak peaks at $d =$ 2.59 and 2.30 nm in a small-angle region. These peaks suggest the formation of a 2D mesochannel array close to hexagonal packing, which is due to the d-spacing ratio of about $1:1/\sqrt{3}:1/2$. The broad diffraction at around $d = 0.41$–0.42 nm is due to the amorphous structure of the siloxane moieties, although the d value is slightly shorter than that of conventional PMOs ($d = 0.44$ nm).[13–20] Interestingly, the mesostructured PBI–silica hybrids showed a molecular-scale periodicity, at $d = 0.36$ and 0.34 nm for PBI-3Pn-PMO-am and PBI-MEE-PMO-am, respectively, corresponding to a typical π–π stacking distance for PBIs. These results suggest that the densely embedded PBI moieties within the PMO frameworks form face-to-face π-stacked molecular assemblies. To the best of our knowledge, this is the first example of the production of periodic mesostructured organosilica materials with a parallel π-stacked organosilica hybrid framework. The introduction of the MEE substituent, showing higher hydrophilicity and less steric hindrance than the 3Pn substituent, onto the imide group leads to the formation of more highly ordered organosilica hybrid structures on the mesoscopic and molecular scales.

The template surfactant in the as-made materials was removed by solvent extraction to give mesoporous PBI–silica hybrids. First, the as-made hybrids were washed with ethanol without post-treatment. However, the mesostructures collapsed after removal of the template. ^{29}Si magic-angle-spinning (MAS) NMR measurements showed that the as-made hybrids were cross-linked by poorly-condensed T^1 and T^2 species (T^n: R-$Si(OSi)_n(OH)_{3-n}$) with the degree of condensation of ca. 50% (Supporting Information, Figure S8). It is likely that the formation of the organosilica hybrid framework, dominated by the π–π stacking nature of the large PBI moieties, hinders efficient condensation and cross-linking of the silyl groups. Extraction of the template surfactant without collapse was realized by reinforcing the PBI–silica frameworks with a pure silica coating. After treatment with acetic acid, the mesostructured hybrids were exposed to tetraethoxysilane (TEOS) vapor for 2–12 h at 120 °C, and the template was then washed out with ethanol. The mesoporous hybrid based on 3Pn-substituted PBI (denoted as PBI-3Pn-PMO-ex) was obtained by extraction of the template after two-hour exposure to TEOS vapor. In contrast, the preparation of mesoporous hybrids based on MEE-substituted PBI required more than six-hour exposure to TEOS vapor; the most successful synthesis of PMO (PBI-MEE-PMO-ex) was realized by reinforcement of the framework for 12 h. The increase in the degree of condensation without disturbing the periodic mesostructures was confirmed by ^{29}Si MAS NMR and XRD measurements (Supporting Information, Figures S8 and S10). The TEOS vapor predominantly reacted with T^1 species, mainly resulting in more condensed T^2 and Q^3 (Q^n: $Si(OSi)_n(OH)_{4-n}$) species (Supporting Information, Figure S8). The T/Q atomic ratios were ca. 1:1 and 1:3 for 2 h and 12 h TEOS treatment, respectively. The XRD patterns (Figure 2 a,b) show that the extracted PBI-bridged PMOs had periodic mesostructures with d-spacing values of about 4 nm. The slight decrease in the d values is due to contraction of the framework through TEOS treatment and extraction of the template. The π–π stacking periodicity within the pore walls was maintained after extraction of the template. ^{13}C cross-polarization MAS NMR measurements of the PBI-bridged PMOs confirmed that the PBI bridging groups were intact after all the post-treatments (Supporting Information, Figure S9).

The porosity of the PBI-bridged PMOs was examined by nitrogen adsorption–desorption isotherms (Supporting Information, Figure S11). The isotherms were close to type I, which is probably due to the small mesopores. The Brunauer–

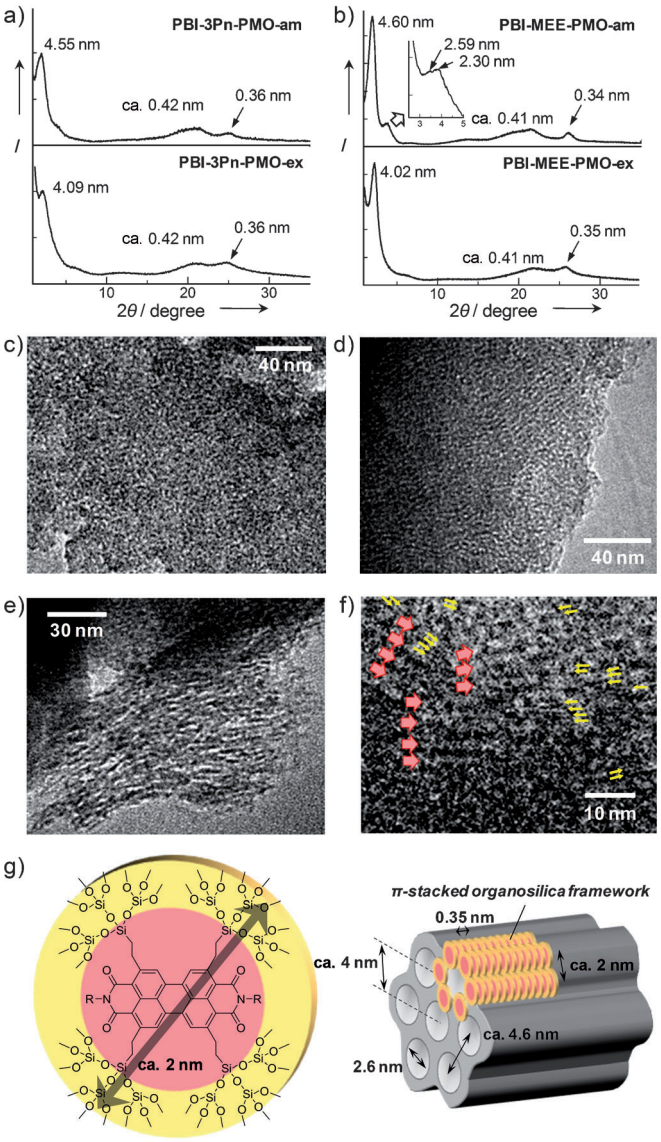

Figure 2. XRD patterns of a) PBI-3 Pn-PMO and b) PBI-MEE-PMO before (top) and after (bottom) extraction of the template surfactant. c) TEM image of PBI-3 Pn-PMO-ex. d)–f) TEM images of PBI-MEE-PMO-ex. Red and yellow arrows in (f) indicate the periodic mesostructures and string-like substructures, respectively. g) Illustration of a PBI-silica disk with a T/Q ratio of 1:3 (left) and structural model of PBI-bridged PMO with π-stacked framework (right).

Emmett–Teller (BET) surface area, pore volume, and DFT pore diameter for PBI-3Pn-PMO-ex were calculated to be 663 $m^2 g^{-1}$, 0.29 $cm^3 g^{-1}$, and 2.6 nm, respectively, whereas for PBI-MEE-PMO-ex, these values were 609 $m^2 g^{-1}$, 0.25 $cm^3 g^{-1}$, and 2.6 nm, respectively. The smaller surface area and pore volume of PBI-MEE-PMO-ex are probably due to the larger amount of silica coating. The contraction of the mesostructures by the post-treatments also led to the formation of small mesopores.

The nanostructures of the PBI-bridged PMO powders were further examined by transmission electron microscopy (TEM). PBI-3Pn-PMO-ex showed a wormhole-like disordered array of mesochannels (Figure 2c). The width of the pores, observed as bright regions in the images, is 2–3 nm, which is in good agreement with the nitrogen isotherm results. For PBI-MEE-PMO-ex, along with wormhole-like regions (Figure 2d), ordered mesochannel arrays were observed (Figure 2e). The periodicity of the mesostructure was about 4–5 nm, which was in agreement with the XRD results. The observed diameter of the mesopores was 2–3 nm. Moreover, string-like substructures with a periodicity of 1.5–2.0 nm were partially observed for PBI-MEE-PMO-ex (Figure 2f; Supporting Information, Figure S13). The string-like architecture presumably corresponds to the π-stacked columnar assemblies of the PBI units. The PBI columns seem to run along the direction of the mesochannels. The formation of columnar PBI assemblies was also supported by XRD and TEM results of a non-porous PBI–silica hybrid prepared by extraction of the template surfactant from PBI-MEE-PMO-am without TEOS treatment (Supporting Information, Figure S14). This sample exhibited a new XRD peak at $d = 1.9$ nm without losing its original π–π stacking periodicity. The TEM image of the non-porous material showed the formation of a 2 nm-thick string-like pattern similar to that of PBI-MEE-PMO-ex; therefore, the organosilica framework likely consists of an array of π-stacked PBI–silica hybrid columns.

The hierarchical structures of the mesoporous PBI–silica hybrids were modeled by considering the mesoscale and molecular-scale periodicities and the size of the molecular components (Figure 2g). The mesoscale periodicities, obtained by XRD measurements, were about 4 nm (d_{100}), which meant that the diameter of the cylindrical structure ($d_{100} \times 2/\sqrt{3}$) was about 4.6 nm, assuming a 2D hexagonal structure. The pore diameters were calculated to be 2.6 nm from the nitrogen isotherms; therefore, the wall thickness was about 2 nm. This value was in good agreement with the thickness of π-stacked PBI–silica hybrid columns with silica coatings. These results indicated that the pore walls of the mesoporous PBI–silica hybrids consisted of one layer of an array of π-stacked PBI–silica columns. Moreover, the correlation length (ξ) of the π-stacking structures was estimated from the peak widths of the XRD profiles at $2\theta = 22$–$28°$ using the Scherrer equation ($\xi = 0.89\lambda/(\omega_{1/2}\cos\theta_0)$; λ = wavelength (1.542 Å); $\omega_{1/2}$ = full width at half-maximum of the diffraction peak; θ_0 = Bragg angle at the maximum), as performed for discotic liquid-crystal materials.[24] The values of ξ for PBI-3Pn-PMO-ex and PBI-MEE-PMO-ex were calculated to be 4.11 (ca. 11-molecule stack) and 5.53 nm (ca. 16-molecule stack), respectively. These values were comparable to conventional discotic liquid crystals[24] and sufficiently larger than the wall thickness so as to suggest that the π-stacked PBI–silica columns lie along the mesochannels. Based on these considerations and the TEM results, a structural model of the PBI-bridged PMOs is shown in Figure 2g. This structure is reasonable because effective ionic interactions between the cationic head groups of the template surfactant and the anionic silanolate species at the surface of the π-stacked PBI columns are rationalized during the surfactant-directed self-assembly process.

The optical properties of the PBI-PMOs were examined by UV/Vis spectroscopy (Figure 3a). As a reference sample, we prepared an amorphous hybrid (PBI-3Pn-Amorph) by

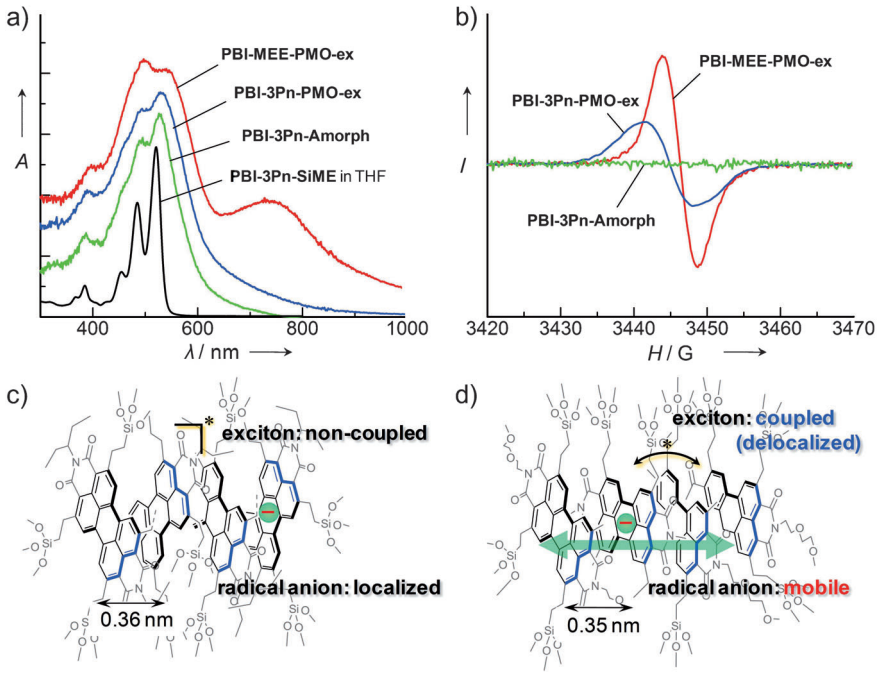

Figure 3. a) UV/Vis spectra of PBI-3Pn-PMO-ex, PBI-MEE-PMO-ex, PBI-3Pn-Amorph, and a solution of the precursor PBI-3Pn-SiME in THF. b) ESR spectra of PBI-3Pn-PMO-ex, PBI-MEE-PMO-ex, and PBI-3Pn-Amorph in saturated hydrazine vapor. c),d) The π-stacking structure of the framework of PBI-3 Pn-PMO (c) and PBI-MEE-PMO (d).

polymerizing PBI-3Pn-SiME in an aqueous solution of NH_3 by macroscopic gelation. The amorphous sample (xerogel consisting of a PBI–silica network) showed no XRD peaks but had a high BET surface area of 801 $m^2 g^{-1}$. PBI-3Pn-PMO-ex showed a similar UV/Vis spectral shape to PBI-3Pn-Amorph and a dilute solution of its precursor (PBI-3Pn-SiME), although the peaks were broadened, indicating that exciton coupling among the PBI units was weak or absent. This suggested that the 3Pn-substituted PBI units in the PMO framework formed a face-to-face stacking structure but with orthogonal transition dipole moments (that is, molecular axes; Figure 3c). This is reasonable because the bulky 3Pn groups are likely to promote an orthogonal arrangement of the PBI units to avoid steric hindrance. In contrast, PBI-MEE-PMO-ex showed a spectral shape dissimilar to a dilute solution of its precursor: the absorption maximum wavelength (λ_{max}) of PBI-MEE-PMO-ex (498 nm) was much shorter than that of the precursor solution ($\lambda_{max} = 521$ nm in THF), accompanied by the appearance of a pronounced shoulder at a longer wavelength ($\lambda \approx 540$ nm). Similar spectral shapes were reported for columnar nanoaggregates of PBI derivatives with exciton coupling between the PBI units.[22] The hypsochromic shift of λ_{max} and the appearance of a new band in the longer wavelength region are rationalized by the molecular exciton theory[25] and are indicative of close face-to-face stacking of rotationally displaced chromophores.[22c,d] These results indicate that π-stacked PBI chromophores with MEE substituents are exciton-coupled; that is, the photoexcited state within the pore walls is delocalized over two or more PBI units (Figure 3d). On the other hand, the broad absorption at $\lambda = 600$–850 nm was assigned as the charge transfer (CT) band of the electron-deficient PBI and the electron-donating silanol or silicate anion groups with electron-rich oxygen atoms. Although the CT bands were observed for both the as-made PMO hybrids, their intensity changed significantly with post-treatment (Supporting Information, Figure S17). The residual CT band of PBI-MEE-PMO-ex was due to the larger amount of silica coating compared to PBI-3Pn-PMO-ex.

The electronic properties of PBI-3Pn-PMO-ex, PBI-MEE-PMO-ex, and PBI-3Pn-Amorph were examined by electron spin-resonance (ESR) spectroscopy (Figure 3b). Measurements were conducted in saturated hydrazine vapor for electron doping at room temperature (vapor pressure: 5 mmHg at 25 °C). The PBI-PMOs showed clear ESR signals attributable to PBI anionic radicals, whereas PBI-3Pn-Amorph showed no detectable ESR signals despite its high surface area. The concentrations of radical spins in PBI-3Pn-PMO-ex and PBI-MEE-PMO-ex were calculated to be 1.37×10^{18} and 1.46×10^{18} spins g^{-1}, respectively, corresponding to 0.27 and 0.42 mol% doping, respectively. The efficiency of electron doping is in the order PBI-MEE-PMO-ex > PBI-3Pn-PMO-ex ≫ PBI-3Pn-Amorph. This electron-accepting behavior cannot be explained based on the surface area. Compared with isolated PBI molecules with discrete HOMO and LUMO levels, the π-stacked one-dimensional assemblies of PBI bridges in the pore walls should have band-like structures with certain bandwidths for valence and conduction bands according to the intermolecular transfer integrals of the HOMOs and LUMOs.[26] In this case, the bottom of the conduction band is lower than the LUMO level of the isolated PBI, which contributes to stabilization of the resultant anionic radicals in the π-stacked PBI–silica framework. The ESR spectral shapes of the PBI-bridged PMOs were indicative of the different electronic states of the PBI anionic radicals (Figure 3b). The peak-to-peak linewidth (ΔH_{pp}) was 7.0 G for PBI-3Pn-PMO-ex and 4.9 G for PBI-MEE-PMO-ex, while the ΔH_{pp} for the PBI anionic radical of the precursors in dilute solution was 4.4 G (Supporting Information, Figure S16). Although the ΔH_{pp} for PMOs is apt to increase due to inhomogeneity of the powder samples, the large difference in ΔH_{pp} of the two PMOs reflects the local environments of the PBI radicals. The smaller ΔH_{pp} of doped PBI-MEE-PMO-ex is attributable to hopping or delocalization of the unpaired electron over several electron-accepting PBI sites, as reported for doped PBI assemblies,[27,28] while the broader ESR spectrum of doped PBI-3Pn-PMO-ex suggests localization of anionic radicals in the inhomogeneous PBI–silica framework (Figure 3c,d). It is reasonable that electron hopping occurs in the pore wall of PBI-MEE-PMO-ex with more

ordered face-to-face association and strong electronic coupling of the PBI moieties. Charge migration in the framework of PBI-MEE-PMO-ex along the PBI columns wrapped with insulating silica layers may contribute to efficient charge separation between the electron donors and the PBI units, stabilization of radicals, and suppression of undesired charge recombination.

In conclusion, a new class of molecularly ordered PMOs with π-stacked framework were synthesized from the disk-like PBI precursors. The PBI-PMOs showed significant potential for transporting charge carriers, excitons, and spins within the framework. It is of great interest that the molecular-scale ordering of disk-like bridges within the PMO framework led to enhancement of the charge-injection efficiency with hydrazine doping and the delocalization or hopping of charges. This remarkable behavior of the PBI-based mesoporous framework should result in innovations in the design of efficient solid-state catalysts and high-performance electronic devices. The synthesis strategy, which consisted of surfactant-directed mesoscale self-assembly of silicate compounds and π-stacking-directed molecular-scale self-assembly of the organic moieties, is applicable to the development of a wide variety of photofunctional and electroactive discotic materials.

Received: July 31, 2011
Revised: October 27, 2011
Published online: December 23, 2011

Keywords: hybrid materials · mesoporous materials · organosilica · π stacking · self-assembly

[1] a) F. Hoffmann, M. Cornelius, J. Morell, M. Fröba, *Angew. Chem.* **2006**, *118*, 3290 – 3328; *Angew. Chem. Int. Ed.* **2006**, *45*, 3216 – 3251; b) F. Hoffmann, M. Fröba, *Chem. Soc. Rev.* **2011**, *40*, 608 – 620.
[2] S. Inagaki, S. Guan, Y. Fukushima, T. Ohsuna, O. Terasaki, *J. Am. Chem. Soc.* **1999**, *121*, 9611 – 9614.
[3] B. J. Melde, B. T. Holland, C. F. Blanford, A. Stein, *Chem. Mater.* **1999**, *11*, 3302 – 3308.
[4] T. Asefa, M. J. MacLachlan, N. Coombs, G. A. Ozin, *Nature* **1999**, *402*, 867 – 871.
[5] W. Wang, J. E. Lofgreen, G. A. Ozin, *Small* **2010**, *6*, 2634 – 2642.
[6] N. Mizoshita, T. Tani, S. Inagaki, *Chem. Soc. Rev.* **2011**, *40*, 789 – 800.
[7] M. Cornelius, F. Hoffmann, B. Ufer, P. Behrens, M. Fröba, *J. Mater. Chem.* **2008**, *18*, 2587 – 2592.
[8] M. A. Wahab, S. Sudhakar, E. Yeo, A. Sellinger, *Chem. Mater.* **2008**, *20*, 1855 – 1861.
[9] a) T. P. Nguyen, P. Hesemann, P. Gaveau, J. J. E. Moreau, *J. Mater. Chem.* **2009**, *19*, 4164 – 4171; b) S. El Hankari, B. Motos-Pérez, P. Hesemann, A. Bouhaouss, J. J. E. Moreau, *J. Mater. Chem.* **2011**, *21*, 6948 – 6955; c) S. El Hankari, B. Motos-Pérez, P. Hesemann, A. Bouhaouss, J. J. E. Moreau, *Chem. Commun.* **2011**, *47*, 6704 – 6706.
[10] a) N. Mizoshita, M. Ikai, T. Tani, S. Inagaki, *J. Am. Chem. Soc.* **2009**, *131*, 14225 – 14227; b) N. Mizoshita, K. Yamanaka, T. Shimada, T. Tani, S. Inagaki, *Chem. Commun.* **2010**, *46*, 9235 – 9237.
[11] a) S. Gu, M. Jaroniec, *J. Mater. Chem.* **2011**, *21*, 6389 – 6394; b) E.-B. Cho, O. H. Han, S. Kim, D. Kim, M. Jaroniec, *Chem. Commun.* **2010**, *46*, 4568 – 4570.
[12] S. E. Dickson, C. M. Crudden, *Chem. Commun.* **2010**, *46*, 2100 – 2102.
[13] S. Inagaki, S. Guan, T. Ohsuna, O. Terasaki, *Nature* **2002**, *416*, 304 – 307.
[14] M. P. Kapoor, Q. Yang, S. Inagaki, *J. Am. Chem. Soc.* **2002**, *124*, 15176 – 15177.
[15] A. Sayari, W. Wang, *J. Am. Chem. Soc.* **2005**, *127*, 12194 – 12195.
[16] M. Cornelius, F. Hoffmann, M. Fröba, *Chem. Mater.* **2005**, *17*, 6674 – 6678.
[17] Y. Xia, W. Wang, R. Mokaya, *J. Am. Chem. Soc.* **2005**, *127*, 790 – 798.
[18] N. Mizoshita, Y. Goto, M. P. Kapoor, T. Shimada, T. Tani, S. Inagaki, *Chem. Eur. J.* **2009**, *15*, 219 – 226.
[19] M. Beretta, J. Morell, P. Sozzani, M. Fröba, *Chem. Commun.* **2010**, *46*, 2495 – 2497.
[20] M. Waki, N. Mizoshita, T. Ohsuna, T. Tani, S. Inagaki, *Chem. Commun.* **2010**, *46*, 8163 – 8165.
[21] a) W. Pisula, X. Feng, K. Müllen, *Adv. Mater.* **2010**, *22*, 3634 – 3649; b) A. Wicklein, A. Lang, M. Muth, M. Thelakkat, *J. Am. Chem. Soc.* **2009**, *131*, 14442 – 14453.
[22] a) N. Mizoshita, T. Tani, S. Inagaki, *Adv. Funct. Mater.* **2011**, *21*, 3291 – 3296; b) F. Würthner, M. Stolte, *Chem. Commun.* **2011**, *47*, 5109 – 5115; c) X.-Q. Li, V. Stepanenko, Z. Chen, P. Prins, L. D. A. Siebbeles, F. Würthner, *Chem. Commun.* **2006**, 3871 – 3873; d) F. Würthner, Z. Chen, V. Dehm, V. Stepanenko, *Chem. Commun.* **2006**, 1188 – 1190.
[23] S. Nakazono, Y. Imazaki, H. Yoo, J. Yang, T. Sasamori, N. Tokitoh, T. Cédric, H. Kageyama, D. Kim, H. Shinokubo, A. Osuka, *Chem. Eur. J.* **2009**, *15*, 7530 – 7533.
[24] P. H. J. Kouwer, O. van den Berg, W. F. Jager, W. J. Mijs, S. J. Picken, *Macromolecules* **2002**, *35*, 2576 – 2582.
[25] M. Kasha, H. R. Rawls, M. A. El-Bayoumi, *Pure Appl. Chem.* **1965**, *11*, 371 – 392.
[26] G. Saito, Y. Yoshida, *Bull. Chem. Soc. Jpn.* **2007**, *80*, 1 – 137.
[27] a) T. M. Wilson, T. A. Zeidan, M. Hariharan, F. D. Lewis, M. R. Wasielewski, *Angew. Chem.* **2010**, *122*, 2435 – 2438; *Angew. Chem. Int. Ed.* **2010**, *49*, 2385 – 2388; b) Y. Che, A. Datar, X. Yang, T. Naddo, J. Zhao, L. Zang, *J. Am. Chem. Soc.* **2007**, *129*, 6354 – 6355; c) S.-G. Chen, H. M. Branz, S. S. Eaton, P. C. Taylor, R. A. Cormier, B. A. Gregg, *J. Phys. Chem. B* **2004**, *108*, 17329 – 17336.
[28] J. R. Norris, R. A. Uphaus, H. L. Crespi, J. J. Katz, *Proc. Natl. Acad. Sci. USA* **1971**, *68*, 625 – 628.

